Ultrafast Triplet Generation at the Lead Halide Perovskite/Rubrene Interface

Carl R. Conti III, [1,#] *Alexander S. Bieber,* [1,#] *Zachary A. VanOrman,* [1] *Gregory Moller,* [1] *Sarah Wieghold,*[1,2,3] *Richard D. Schaller,*[2] *Geoffrey F. Strouse,*[1] *Lea Nienhaus*[1,*]

[1]Department of Chemistry and Biochemistry, Florida State University, Tallahassee, FL 32306, USA

[2]Center for Nanoscale Materials, Argonne National Laboratory, Lemont, IL 60439, USA

[3]Advanced Photon Source, Argonne National Laboratory, Lemont, IL 60439, USA

[#]equal contribution

*corresponding Author: lnienhaus@fsu.edu

ABSTRACT

Triplet sensitization of rubrene by bulk lead halide perovskites has recently resulted in efficient infrared-to-visible photon upconversion *via* triplet-triplet annihilation. Notably, this process occurrs under solar relavant fluxes, potentially paving the way toward integration with photovoltaic devices. In order to further improve the upconversion efficiency, the fundamental photophysical pathways at the perovskite/rubrene interface must be clearly understood to maximize charge extraction. Here, we utilize ultrafast transient absorption spectroscopy to elucidate the processes underlying the triplet generation at the perovskite/rubrene interface. Based on the bleach and photoinduced absorption features of the perovskite and perovskite/rubrene devices obtained at multiple pump wavelengths and fluences, along with their resultant kinetics, our results do not support charge transfer states or long-lived trap states as the underlying mechanism. Instead, the data points towards a triplet sensitization mechanism based on rapid extraction of thermally excited carriers on the picosecond timescale.

TOC Graphic

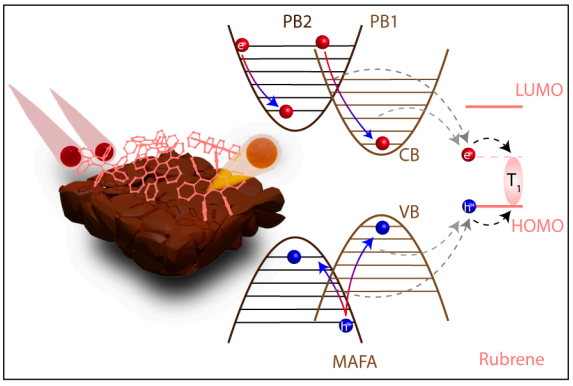

Silicon-based solar cells, the current workhorse of solar energy, cannot absorb wavelengths beyond 1100 nm, limiting the efficient use of the entire solar spectrum.[1–3] A promising approach to overcome this fundamental limitation is the use of photon upconversion (UC).[4–9] Particularly promising is UC *via* triplet-triplet annihilation (TTA) in organic semiconductors, as it can become efficient at solar-relevant incident powers.[10–12] Due to spin selectrion rules, the spin-triplet states required for TTA-UC are populated *via* energy transfer from triplet sensitizers that generate triplet states through intersystem crossing,[8,13,14] inherently exhibit an excitonic wavefunction that possesses both triplet and singlet character,[7,15–18] or through asynchronous charge transfer (CT) processes from bulk lead halide perovskite materials.[12,19–25]

The long free carrier lifetimes, high absorption cross sections and facile bandgap tunability of perovskites,[26–29] which are desirable properties in photovoltaic applications also yield the required foundation for triplet sensitization.[12,19–23] It is established that lead halide perovskites of varying halide and A-site compositions are capable of sensitizing the triplet state of rubrene. However, to date, the exact mechanism of triplet sensitization is still unclear.[30–33] Understanding the fundamental mechanism of triplet sensitization at the perovskite/organic interface will be the key in further improving perovskite-based UC, as it will unlock engineering pathways to further increase the device performance.

We have previously observed a lack of noticeable perovskite photoluminescence (PL) quenching in the presence of rubrene, which was attributed in part to strong back transfer of the upconverted singlets and surface passivation effects.[12,20,22] However, this observation may indicate a more intricate triplet sensitization mechanism than the current simplistic view of direct charge carrier extraction from the perovskite to rubrene (Figure 1a). Particularly, it emphasizes that only a small fraction of free charges created upon photoexcitation are successfully extracted and return

upconverted photons despite the long-lived nature of the free carriers in the perovskite, which should allow a large number of charges to be extracted within their lifetime.[23,28] Possible causes include localized states mediating electron and hole transfer and limiting the number of generated triplet states[30,31] and short-lived transient states (*e.g.* hot carriers) being involved in the triplet generation process.[34] In addition, this simple mechanism does not consider the possible influence of mid-gap trap states or higher energy transitions in the perovskite which may also play a role in the triplet sensitization process.[35–37]

In this contribution, we utilize ultrafast transient absorption (TA) spectroscopy to investigate the photophysical processes occuring at the interface of $MA_{0.85}FA_{0.15}PbI_3$ (MAFA) and rubrene doped with ~1% dibenzotetraphenylperiflanthene (DBP). The resulting bilayer UC devices are denoted as MAFA/rub in the following (inset Figure 1b). In Figure 1b, the steady-state absorption of the MAFA thin film and MAFA/rub bilayer is shown. The vibronic features of the rubrene/DBP absorption spectrum are highlighted, as well as the region of the two photobleaches (PB1, PB2) commonly observed in TA spectroscopy of lead halide perovskites.[34–36,38,39] The transient absorption data measured under 700 nm (pulse energy: 1.2 mJ/cm^2) excitation is plotted in Figure 1c,d as a temperature plot to allow the time dependent evolution of the absorption features to be visualized. Figure 1e,f shows the extracted absorbance spectra for MAFA and MAFA/rub at different probe time delays under 700 nm excitation and pulse energies of 0.6 mJ/cm^2 and 1.2 mJ/cm^2.

PB1 corresponds to the perovskite ground state bleach at 780 nm, while the origin of PB2 at 485 nm in perovskites is still under debate; PB2 has been attributed to band filling effects stemming from two VBs and a shared CB,[36,39] one shared VB and two CBs,[38,39] or a high energy CT state, which is attributed to an I_2-like species formed under optical excitation.[35] In addition, a

broad photoinduced absorption (PIA1) can be observed between 510-700 nm, which has been assigned to photoinduced refractive index changes or excited state transitions stemming from free carriers.[34,40] A second localized PIA2 is found at 550 nm, which is correlated to PB2, as the recovery kinetics are similar and a clear isosbestic point is found at ~ 514 nm (Figure 1e,f).[35]

In the MAFA/rub device, additional overlapping PIAs are observed at ~ 480 nm, 520 nm, and 550 nm, which correspond to the rubrene triplet excited state $T_1 \rightarrow T_n$ transitions and polaron signature, respectively (compare Figure S1).[41–44] The excited state triplet absorption signal in MAFA/rub confirms the rubrene triplet sensitization under 700 nm excitation. Comparing the TA surfaces of MAFA and MAFA/rub in Figure 1c,d and the extracted spectra in Figure 1e,f, we find no additional unexpected absorbing features in the presence of rubrene within the measurement window. Thus, our findings do not support a bound interfacial CT state as the underlying mechanism. In addition, no signature of a long-lived (*e.g.*, defect-related) state within the spectral window of the measurement is found.

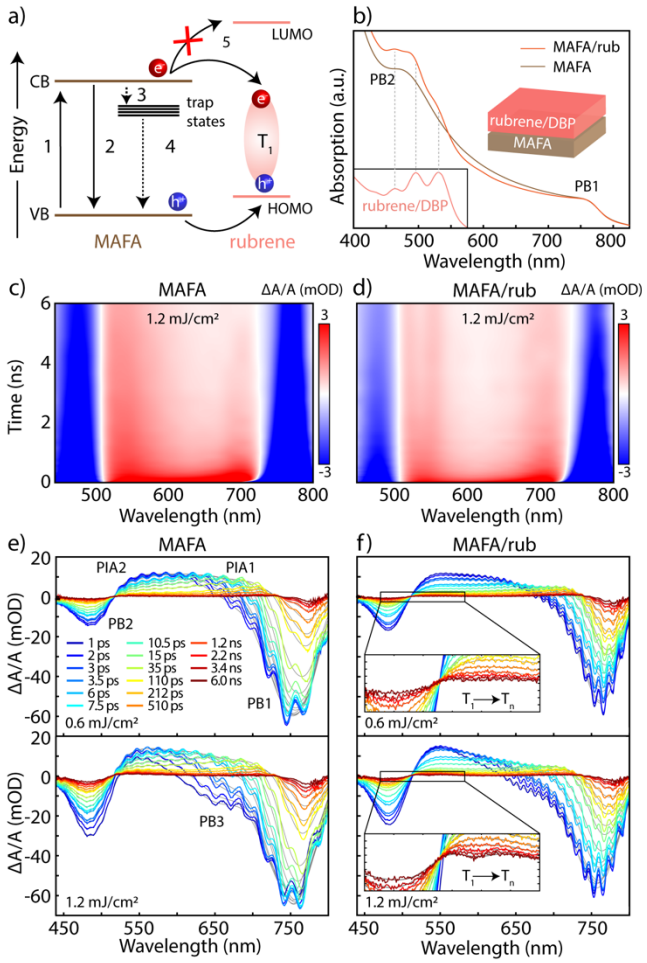

Figure 1: (a) Schematic of the rubrene sensitization mechanism. (1) Photon absorption promotes an electron from the VB to the CB of the perovskite. This excited state can relax to the ground state via several pathways: (2) free carrier recombination, (3) charge trapping at shallow defect levels and relaxation by (4) trap-assisted charge carrier recombination, or (5) charge transfer to the triplet state of rubrene. (b) Absorbance spectra of MAFA and MAFA/rub. The spectral regions of the two photobleaches observed in TA are labeled with PB1 and PB2. The inset shows the absorption spectra of a rubrene/DBP film. (c) TA surface of MAFA and (d) MAFA/rub under 700 nm pump at a pulse power of 1.2 mJ/cm^2. To remove the strong etalon feature, the TA surfaces were processed with a frequency filter. (e,f) Absorbance spectra at selected delay times for MAFA (e) and MAFA/rub (f) at 0.6 mJ/cm^2 (top) and 1.2 mJ/cm^2 (bottom) pulse power. The gray lines depict the frequency-filtered data. The inset highlights the PIA feature corresponding to the $T_1 \rightarrow T_n$ transition of rubrene at 521 nm and polaron feature at 553 nm.

Further analysis of the TA data in Figure 1 reveals that PB2 exhibits distinctly different dynamics than PB1,[35] and both PB levels recover more rapidly in the presence of rubrene (*vide infra*). Similarly, PIA2 is reduced more rapidly. Therefore, the data indicates that the carriers populating the electronic states of this higher excited state may play a role in the UC process. It has been suggested that the PB2 state is populated by either direct absorption, a hot carrier/phonon-

based mechanism or an Auger-based population of the high energy state.[35,38] To determine if the population of PB2 influences the triplet generation process, we investigate the response of MAFA and MAFA/rub to different wavelengths and different excitation powers. Broad absorption should reveal an excitation wavelength-dependent population of the higher energy state, while to first approximation, the ratio of bleach of PB1 and PB2 should not be affected. On the other hand, both phonon-assisted or Auger-type mechanisms are expected to be excitation wavelength and fluence-dependent.

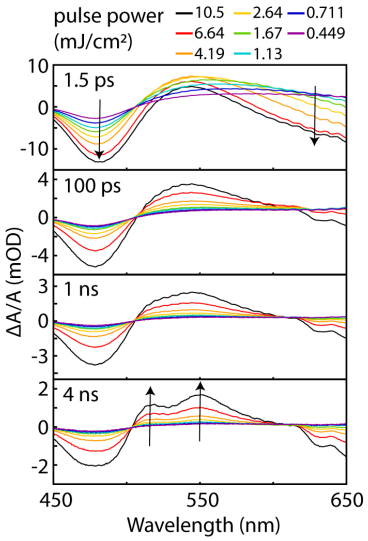

Figure 2: MAFA/rub absorbance spectra at power densities ranging from 1.13 mJ/cm^2 to 10.5 mJ/cm^2 obtained at delay times of 1.5 ps, 100 ps, 1 ns and 4 ns. All spectra were recorded under 700 nm excitation. The arrows are guides to the eye to highlight the increase in the PBs at higher powers and the growth of the rubrene triplet-related PIA.

The absorbance spectra of MAFA/rub for a wider range of pump energies (1.13 mJ/cm^2 to 10.5 mJ/cm^2) at selected delay times of 1.5 ps, 100 ps, 1 ns and 4 ns for MAFA/rub are shown in Figure 2, clearly showing the grow-in of the characteristic rubrene $T_1 \rightarrow T_n$ triplet excited state absorption, as well as the polaron signature at 553 nm.

Based on the data presented in Figure 1 and Figure 2, we establish the following: i) At higher excitation fluence and higher photon energy, an additional short-lived broad bleach signature (PB3) can be observed (compare Figure S2 for 808 nm and S3 for 400 nm and 650 nm

excitation), and rapidly decays as PB1 is populated (Figure S4). In agreement with previous work, we attribute this absorbing species to thermally excited (hot) carriers rapidly cooling to the lower energy band edge.[40,45–48] PB3 is more pronounced in MAFA than MAFA/rub, indicating that the interaction between rubrene and the perovskite surface reduces the presence of this absorbing species, suggesting that hot charge carriers are directly extracted to rubrene.[34] ii) The intensity of PIA1 is reduced in the presence of rubrene, emphasizing the features of the localized PIA2. We find PIA1 initially redshifts rapidly due to the dynamic Burstein-Moss effect.[36,39] Up to ~200 ps, the spectral shape continues to evolve due to Auger relaxation,[39,49] after which PIA1 converges to a uniform spectral shape, with a clear isosbestic point at 730 nm. iii) PB2 is populated prior to PB1, and the bleach intensity of PB2 depends both on photon energy and pulse power. PB2 (2.56 eV) is populated under excitation at 808 nm (1.53 eV), which is below the optical bandgap of MAFA (1.59 eV), suggesting PB2 is not populated by direct absorption. Therefore, we suggest that the generation of PB2 is based on hot carriers: either by direct thermal excitation *via* phonons or a Auger-based hot carrier relaxation. iv) For both MAFA and MAFA/rub, PB1 is narrower at lower pulse power and photon energy, further highlighting the effect of hot carriers on the TA spectra (*vide infra*). v) The emergence of the rubrene triplet-related PIA is both excitation wavelength and fluence dependent. Interestingly, there is no direct correlation to the intensity of PB1, which is related to the population of the band edge excited state. However, there is a relationship between the triplet PIA and the intensity of PIA2, PB2, and PB3, indicating a relationship between the population of the higher energy bleach features and the successful generation of the triplet state. vi) No PbI_2-related signature is found (Figure S5), ruling out the role of PbI_2 as a mediating factor for triplet sensitization.

We have previously established that the power dependence of perovskite-sensitized TTA-UC is dependent on the underlying perovskite recombination dynamics, and does not simply exhibit the characteristic quadratic-to-linear trend of TTA.[12] The observed non-linear dependence of the triplet formation on the excitation power further confirms this observation and indicates that triplet formation is not simply proportional to the number of incident photons. By extracting the triplet-related PIA from the residual underlying perovskite PIA2, we find a superlinear growth ($\alpha \approx 1.5$) of the triplet state based on incident power (Figure S6).

To shed more light onto the underlying mechanism of triplet sensitization, we investigate the kinetics under 700 nm excitation (1.2 mJ/cm^2) at the MAFA ground state bleach (PB1, 780 nm) and the related PIA1 (700 nm), as shown in Figure 3a. The dynamics of PB1 are well fit by a triexponential function with an offset, which is required since PB1 does not fully recover within the measurement window:

$$\Delta A/A(t) = A_1 \exp\left(-\frac{t}{\tau_1}\right) + A_2 \exp\left(-\frac{t}{\tau_2}\right) + A_3 \exp\left(-\frac{t}{\tau_3}\right) + A_4. \quad (1)$$

The characteristic time constants are listed in Table 1 for MAFA and MAFA/rub. We find that in the first 20 ps PB1 rapidly recovers in the presence of rubrene, indicating ultrafast charge extraction from the perovskite to rubrene. However, at later times, the dynamics slow and the underlying MAFA kinetics are recovered, indicating a population of carriers that are unaffected by the addition of rubrene, which we have previously attributed to charges in the bulk of the perovskite that do not reach the interface prior to recombination.[19,23]

Table 1: Amplitudes (A) and decay time components (τ) for PB1. A_4 corresponds to an infinite time constant, as PB1 does not fully decay within our measurement window.

	A_1	τ_1(ps)	A_2	τ_2(ps)	A_3	τ_3(ps)	A_4
MAFA	0.37	46	0.28	185	0.30	1063	0.10
MAFA/Rub	0.49	8.9	0.27	165	0.27	999	0.09

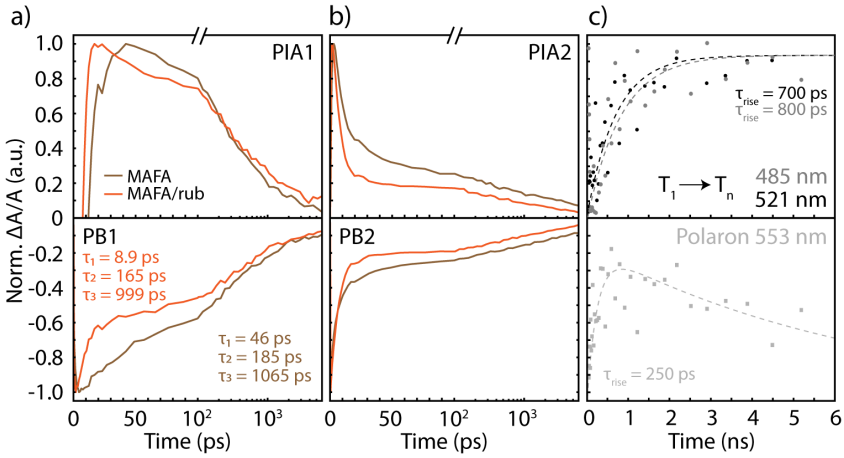

Figure 3: Normalized TA dynamics under 700 nm excitation at a power density of 1.2 mJ/cm^2 for MAFA and MAFA/rub. The dynamics were extracted at (a) PIA1 (top), PB1 (bottom) and (b) PIA2 (top), PB2 (bottom). The corresponding wavelengths of the spectral features are 700 nm (PIA1), 780 nm (PB1), 553 nm (PIA2) and 485 nm (PB2), respectively. (c) The extracted kinetics for the overlaying rubrene $T_1 \rightarrow T_n$ trasnsitions at 485 nm (gray) and 521 nm (black) and polaron PIA at 553 nm (light gray). We extract a rise time of τ_{rise} = 700 ps and τ_{rise} = 800 ps for the triplet $T_1 \rightarrow T_n$ transitions at 521 nm and 485 nm, respectively. The polaron has a characteristic rise time of τ_{rise}=250 ps and begins to decay within the measurement window.

PIA1 grows in more rapidly for MAFA/rub than MAFA, initially recovers faster, and then appears to stagnate at later times. This is the result of multiple factors. First, the overlapping PB3 recovers more rapidly in the presence of rubrene (Figure S4). Second, PIA1 is correlated to PB1, and ultrafast charge extraction results in a faster initial recovery. Third, formation of rubrene polarons can result in a long-lived overlapping PIA, as charged rubrene species exhibit PIA in the spectral region between 520 – 900 nm,[50] which would effectively prolong the signal detected at this wavelength.

We also find a faster recovery of both PB2 and PIA2 in the presence of rubrene (Figure 3b), indicating this higher energy state is also influenced by the presence of rubrene. However, we cannot conclusively determine whether the state is directly quenched or the quenching is a result of an equilibrium with PB1, which is rapidly depopulated by the presence of rubrene. Yet, as evidenced by our power-dependent TA spectra (Figure S6), a clear correlation exists between the

initial population of this state and a high yield of triplet generation, which indicates that the same charge carriers which populate PB2 also generate the triplet state of rubrene.

To determine the rate of triplet generation, we take a closer look at the recombination dynamics of PB2 and PIA2, as the triplet PIA is overlapping in this region (see Supporting Information, Figure S7). The resulting extracted triplet kinetics are well fit by a rise time of τ_{rise} = 700 ps for the $T_1 \rightarrow T_n$ transition at 521 nm and τ_{rise} = 800 ps for the $T_1 \rightarrow T_n$ transition at 485 nm (Figure 3c, top), and further highlight the expected persistence of the triplets beyond our measurement window. The polaron-related PIA at 550 nm is similarly fit with a rise time of τ_{rise} = 250 ps (Figure 3c, bottom), and begins to decay within our measurement window. We attribute this to triplet formation through the polaron state,[43,51] which is further supported by the increased intensity of the rubrene polaron feature relative to the $T_1 \rightarrow T_n$ transition in MAFA/rub than in the rubrene thin film (Figure S1b) and the visible decay of the polaron state within our measurement window.

The proposed excited state steps involved in the triplet generation in MAFA/rub are summarized in Figure 4, where the more rapid recovery of PB1 is attributed to charge extraction to rubrene. PB2 and the related PIA2 are also quenched, indicating that this higher energy transition in the perovskite also plays a role in the triplet sensitization mechanism. Specifically, we propose that the thermally excited carriers that populate PB2 are extracted to rubrene and form the bound triplet state. The additional PB3 observed in MAFA is reduced in MAFA/rub, emphasizing a change in the hot carrier properties upon addition of the organic molecules.

Our results therefore suggest that PB2 and PB3 are populated by a hot-carrier-based mechanism, and carrier extraction from MAFA to rubrene occurrs rapidly while the charge carriers are thermally excited. Upon photoexcitation, hot carriers are generated which rapidly thermalize

via elastic carrier-carrier scattering. Once equilibrated, hot carriers occupy states according to a Fermi-Dirac distribution with a dynamic quasi-Fermi level.[40,45,46] These hot carriers initially populate the higher excited states PB2 and PB3, from which they can either be extracted directly to the rubrene polaron or triplet state or act as a reservoir to repopulate PB1. Thermally excited charge carriers are directly extracted to rubrene and recombine to the bound triplet state, as evidenced by the more rapid recovery of PB1 at early times, the observed more rapid carrier cooling (*vide infra*), and the emergence of the rubrene polaron and triplet-related PIA (Figure 4a). Once the carriers have thermalized to the band edge, charge transfer to the rubrene triplet state slows down significantly, as the energetic driving force is reduced and subsequent charge transfer may require additional phonon support (Figure 4b).[33]

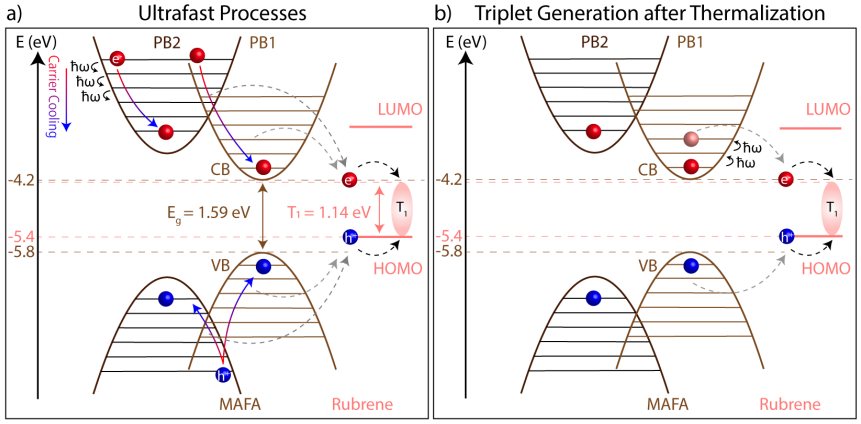

Figure 4: Proposed mechanism of triplet generation in MAFA/rub bilayer devices. (a) Ultrafast processes occurring: optical excitation populates higher excited states. Hot carrier relaxation releases phonons (ħω) and the cooled carriers populate PB2 and the band edge PB1. Thermally excited carriers rapidly transfer to rubrene and combine to form the bound triplet state. (b) Once all carriers are thermalized and populate the band edges of PB1 and PB2 charge extraction to rubrene slows significantly, indicating the possible role of phonon-mediated transfer: phonons excite the carriers to higher excited states, from which charge extraction can occur efficiently.

To support our proposed mechanism and investigate the properties of the hot carriers more fully, we track the carrier temperatures extracted from the TA spectra at different delay times (Figure 5a) and the shift of the quasi-Fermi level (E_F) over time (Figure 5b) under different excitation fluences at 700 nm.[46,52] In agreement with previous reports, we find higher carrier temperatures at high pump fluences, and that the hot-phonon bottleneck effect observed in

perovskite thin films extends the carrier cooling time.[52,53] As expected for hot carrier extraction, in the presence of rubrene, the carrier temperatures for MAFA/rub cool at a faster rate than for MAFA. This is further highlighted by a lower quasi-Fermi level and a redder intital PB1 position for MAFA/rub than MAFA (Figure 5b,c). The effect of the different carrier temperatures can also be observed in the PB1 dynamics. We find that the buildup of PB1 is faster in the presence of rubrene and at lower excitation powers (Figure 5d), in agreement with previous reports on higher carrier temperatures resulting in a slower buildup of the ground state bleach.[34] For an average pulse energy of 1.2 mJ/cm^2 at a pump wavelength of 700 nm, the time constant of the PB1 buildup of MAFA is 1.1 ps and shortens to 0.4 ps for MAFA/rub.

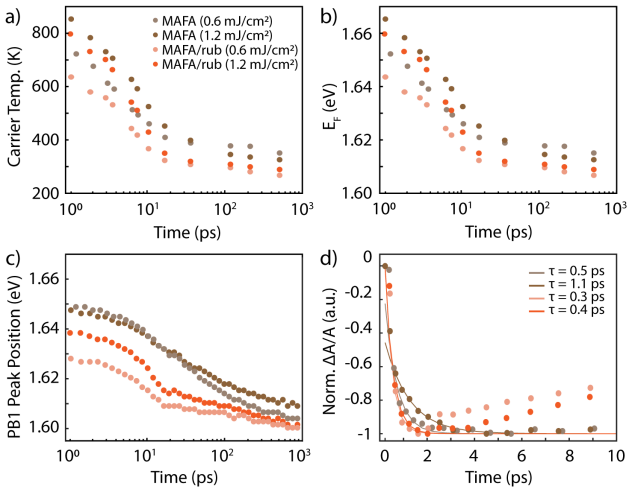

Figure 5: (a) Carrier temperatures at various delay times for MAFA (brown) and MAFA/rub (orange) under 700 nm excitation at pulse fluences of 0.6 mJ/cm^2 and 1.2 mJ/cm^2. (b) The position of the quasi-Fermi level (E_f) as a function of the delay time. (c) Perovskite ground state bleach (PB1) position as a function of time. (d) TA kinetics of MAFA (brown) and MAFA/rub (orange) under 700 nm pump, extracted at the perovskite ground state bleach feature at 780 nm (denoted as PB1, in text). The initial decay is fit (solid line) with an exponential decay function, yielding the time constants shown in the legend.

In summary, we have investigated the MAFA/rubrene interface by means of ultrafast TA spectroscopy. Our results indicate ultrafast charge extraction and subsequent triplet generation on a sub-nanosecond timescale. The PIA at 550 nm has previously been attributed to polarons in rubrene, and is generated at a faster rate than the triplet PIA. The non-linear response of the triplet

generation indicates that the triplet generation does not rely on a simple 'one photon in, one triplet out' mechanism. Rather, it is indicative of the involvement of higher order processes such as non-geminate free carrier recombination or Auger recombination. Our results do not suggest the participation of a localized CT state or long-lived trap states. Therefore, in agreement with our previous results, we emphasize that the key factor for triplet generation is the energetic alignment for charge injection from the VB and CB of the perovskite into the triplet state of rubrene. Our results indicate that a strong population of PB2 and PIA2 yield a strong triplet signature. Hence we propose that the same mechanism that populates PB2 also populates the triplet state, which we attribute to hot carriers. A hot-carrier-based mechanism is further supported by our previous observation that the the perovskite emission is not necessarily quenched in the presence of rubrene: only carriers reaching the interface while they are 'hot' can be efficiently extracted to the triplet state. Despite the long free carrier lifetime of halide perovskites, carriers generated further from the interface would cool prior to reaching the interface, limiting the number of carriers that can be rapidly extracted. However, at later times outside of our observation window, additional carriers can slowly transfer by taking advantage of the rich phonon bath present in perovskite materials.

ASSOCIATED CONTENT

Supporting Information. Details of experimental methods, carrier temperature calculations and additional TA data.

AUTHOR INFORMATION

C.R.C. and A.S.B. contributed equally.

Corresponding Author

*E-mail: lnienhaus@fsu.edu

Notes

FSU has filed a provisional application for a US patent based on this technology that names L.N. and S.W. as inventors.

ACKNOWLEDGEMENTS

A.S.B., Z.A.V., H.K.D., G.M. and L.N. acknowledge funding by Florida State University. C.R.C. and G.F.S. acknowledge the National Science Foundation under Grant No. DMR-1905757. This work was performed, in part, at the Center for Nanoscale Materials, a U.S. Department of Energy Office of Science User Facility, and supported by the U.S. Department of Energy, Office of Science, under Contract No. DE-AC02-06CH11357.

REFERENCES

(1) Green, M. A. High Efficiency Silicon Solar Cells. In *Seventh E.C. Photovoltaic Solar Energy Conference*; Goetzberger, A., Palz, W., Willeke, G., Eds.; Springer Netherlands: Dordrecht, 1987; pp 681–687. https://doi.org/10.1007/978-94-009-3817-5_121.

(2) Swanson, R. M. A Vision for Crystalline Silicon Photovoltaics. *Prog. Photovolt. Res. Appl.* **2006**, *14* (5), 443–453. https://doi.org/10.1002/pip.709.

(3) Trupke, T.; Green, M. A.; Würfel, P. Improving Solar Cell Efficiencies by Up-Conversion of Sub-Band-Gap Light. *J. Appl. Phys.* **2002**, *92* (7), 4117–4122. https://doi.org/10.1063/1.1505677.

(4) Cheng, Y. Y.; Fückel, B.; MacQueen, R. W.; Khoury, T.; Clady, R. G. C. R.; Schulze, T. F.; Ekins-Daukes, N. J.; Crossley, M. J.; Stannowski, B.; Lips, K.; Schmidt, T. W. Improving the Light-Harvesting of Amorphous Silicon Solar Cells with Photochemical Upconversion. *Energy Environ. Sci.* **2012**, *5* (5), 6953–6959. https://doi.org/10.1039/C2EE21136J.

(5) Frazer, L.; Gallaher, J. K.; Schmidt, T. W. Optimizing the Efficiency of Solar Photon Upconversion. *ACS Energy Lett.* **2017**, *2* (6), 1346–1354. https://doi.org/10.1021/acsenergylett.7b00237.

(6) Schmidt, T. W.; Castellano, F. N. Photochemical Upconversion: The Primacy of Kinetics. *J. Phys. Chem. Lett.* **2014**, *5* (22), 4062–4072. https://doi.org/10.1021/jz501799m.

(7) Garakyaraghi, S.; Mongin, C.; Granger, D. B.; Anthony, J. E.; Castellano, F. N. Delayed Molecular Triplet Generation from Energized Lead Sulfide Quantum Dots. *J. Phys. Chem. Lett.* **2017**, *8* (7), 1458–1463. https://doi.org/10.1021/acs.jpclett.7b00546.
(8) Cheng, Y. Y.; Khoury, T.; Clady, R. G. C. R.; Tayebjee, M. J. Y.; Ekins-Daukes, N. J.; Crossley, M. J.; Schmidt, T. W. On the Efficiency Limit of Triplet–Triplet Annihilation for Photochemical Upconversion. *Phys. Chem. Chem. Phys.* **2010**, *12* (1), 66–71. https://doi.org/10.1039/B913243K.
(9) Gholizadeh, E. M.; Prasad, S. K. K.; Teh, Z. L.; Ishwara, T.; Norman, S.; Petty, A. J.; Cole, J. H.; Cheong, S.; Tilley, R. D.; Anthony, J. E.; Huang, S.; Schmidt, T. W. Photochemical Upconversion of Near-Infrared Light from below the Silicon Bandgap. *Nat. Photonics* **2020**, *14* (9), 585–590. https://doi.org/10.1038/s41566-020-0664-3.
(10) Singh-Rachford, T. N.; Castellano, F. N. Photon Upconversion Based on Sensitized Triplet–Triplet Annihilation. *Coord. Chem. Rev.* **2010**, *254* (21), 2560–2573. https://doi.org/10.1016/j.ccr.2010.01.003.
(11) Mahboub, M.; Huang, Z.; Tang, M. L. Efficient Infrared-to-Visible Upconversion with Subsolar Irradiance. *Nano Lett.* **2016**, *16* (11), 7169–7175. https://doi.org/10.1021/acs.nanolett.6b03503.
(12) Wieghold, S.; Bieber, A. S.; VanOrman, Z. A.; Daley, L.; Leger, M.; Correa-Baena, J.-P.; Nienhaus, L. Triplet Sensitization by Lead Halide Perovskite Thin Films for Efficient Solid-State Photon Upconversion at Subsolar Fluxes. *Matter* **2019**, *1* (3), 705–719. https://doi.org/10.1016/j.matt.2019.05.026.
(13) Islangulov, R. R.; Kozlov, D. V.; Castellano, F. N. Low Power Upconversion Using MLCT Sensitizers. *Chem. Commun.* **2005**, No. 30, 3776–3778. https://doi.org/10.1039/B506575E.
(14) Amemori, S.; Sasaki, Y.; Yanai, N.; Kimizuka, N. Near-Infrared-to-Visible Photon Upconversion Sensitized by a Metal Complex with Spin-Forbidden yet Strong S_0–T_1 Absorption. *J. Am. Chem. Soc.* **2016**, *138* (28), 8702–8705. https://doi.org/10.1021/jacs.6b04692.
(15) Nienhaus, L.; Wu, M.; Geva, N.; Shepherd, J. J.; Wilson, M. W. B.; Bulović, V.; Van Voorhis, T.; Baldo, M. A.; Bawendi, M. G. Speed Limit for Triplet-Exciton Transfer in Solid-State PbS Nanocrystal-Sensitized Photon Upconversion. *ACS Nano* **2017**, *11* (8), 7848–7857. https://doi.org/10.1021/acsnano.7b02024.
(16) Wu, M.; Congreve, D. N.; Wilson, M. W. B.; Jean, J.; Geva, N.; Welborn, M.; Van Voorhis, T.; Bulović, V.; Bawendi, M. G.; Baldo, M. A. Solid-State Infrared-to-Visible Upconversion Sensitized by Colloidal Nanocrystals. *Nat. Photonics* **2016**, *10* (1), 31–34. https://doi.org/10.1038/nphoton.2015.226.
(17) Mongin, C.; Garakyaraghi, S.; Razgoniaeva, N.; Zamkov, M.; Castellano, F. N. Direct Observation of Triplet Energy Transfer from Semiconductor Nanocrystals. *Science* **2016**, *351* (6271), 369–372. https://doi.org/10.1126/science.aad6378.
(18) Huang, Z.; Xu, Z.; Mahboub, M.; Li, X.; Taylor, J. W.; Harman, W. H.; Lian, T.; Tang, M. L. PbS/CdS Core–Shell Quantum Dots Suppress Charge Transfer and Enhance Triplet Transfer. *Angew. Chem.* **2017**, *129* (52), 16810–16814. https://doi.org/10.1002/ange.201710224.
(19) VanOrman, Z. A.; Lackner, J.; Wieghold, S.; Nienhaus, K.; Nienhaus, G. U.; Nienhaus, L. Efficiency of Bulk Perovskite-Sensitized Upconversion: Illuminating Matters. *Appl. Phys. Lett.* **2021**, *118* (20), 203903. https://doi.org/10.1063/5.0050185.

(20) Wieghold, S.; Bieber, A. S.; VanOrman, Z. A.; Nienhaus, L. Influence of Triplet Diffusion on Lead Halide Perovskite-Sensitized Solid-State Upconversion. *J. Phys. Chem. Lett.* **2019**, *10* (13), 3806–3811. https://doi.org/10.1021/acs.jpclett.9b01526.
(21) Wieghold, S.; Bieber, A. S.; Lackner, J.; Nienhaus, K.; Nienhaus, G. U.; Nienhaus, L. One-Step Fabrication of Perovskite-Based Upconversion Devices. *ChemPhotoChem* **2020**, *4* (9), 704–712. https://doi.org/10.1002/cptc.202000068.
(22) Wieghold, S.; Nienhaus, L. Precharging Photon Upconversion: Interfacial Interactions in Solution-Processed Perovskite Upconversion Devices. *J. Phys. Chem. Lett.* **2020**, *11* (3), 601–607. https://doi.org/10.1021/acs.jpclett.9b03596.
(23) VanOrman, Z. A.; Nienhaus, L. Bulk Metal Halide Perovskites as Triplet Sensitizers: Taking Charge of Upconversion. *ACS Energy Lett.* **2021**, *6* (10), 3686–3694. https://doi.org/10.1021/acsenergylett.1c01794.
(24) VanOrman, Z. A.; Drozdick, H. K.; Wieghold, S.; Nienhaus, L. Bulk Halide Perovskites as Triplet Sensitizers: Progress and Prospects in Photon Upconversion. *J. Mater. Chem. C* **2021**, *9* (8), 2685–2694. https://doi.org/10.1039/D1TC00245G.
(25) Wieghold, S.; VanOrman, Z. A.; Nienhaus, L. Halide Perovskites: A Progress Report on Photon Interconversion. *Adv. Opt. Mater.* **2021**, *9* (18), 2001470. https://doi.org/10.1002/adom.202001470.
(26) Galkowski, K.; Mitioglu, A.; Miyata, A.; Plochocka, P.; Portugall, O.; Eperon, G. E.; Wang, J. T.-W.; Stergiopoulos, T.; Stranks, S. D.; Snaith, H. J.; Nicholas, R. J. Determination of the Exciton Binding Energy and Effective Masses for Methylammonium and Formamidinium Lead Tri-Halide Perovskite Semiconductors. *Energy Environ. Sci.* **2016**, *9* (3), 962–970. https://doi.org/10.1039/C5EE03435C.
(27) Yang, Y.; Yang, M.; Li, Z.; Crisp, R.; Zhu, K.; Beard, M. C. Comparison of Recombination Dynamics in $CH_3NH_3PbBr_3$ and $CH_3NH_3PbI_3$ Perovskite Films: Influence of Exciton Binding Energy. *J. Phys. Chem. Lett.* **2015**, *6* (23), 4688–4692. https://doi.org/10.1021/acs.jpclett.5b02290.
(28) Stranks, S. D.; Eperon, G. E.; Grancini, G.; Menelaou, C.; Alcocer, M. J. P.; Leijtens, T.; Herz, L. M.; Petrozza, A.; Snaith, H. J. Electron-Hole Diffusion Lengths Exceeding 1 Micrometer in an Organometal Trihalide Perovskite Absorber. *Science* **2013**, *342* (6156), 341–344. https://doi.org/10.1126/science.1243982.
(29) Yamada, Y.; Nakamura, T.; Endo, M.; Wakamiya, A.; Kanemitsu, Y. Photocarrier Recombination Dynamics in Perovskite CH3NH3PbI3 for Solar Cell Applications. *J. Am. Chem. Soc.* **2014**, *136* (33), 11610–11613. https://doi.org/10.1021/ja506624n.
(30) Prashanthan, K.; Naydenov, B.; Lips, K.; Unger, E.; MacQueen, R. W. Interdependence of Photon Upconversion Performance and Antisolvent Processing in Thin-Film Halide Perovskite-Sensitized Triplet–Triplet Annihilators. *J. Chem. Phys.* **2020**, *153* (16), 164711. https://doi.org/10.1063/5.0026564.
(31) Wang, L.; Yoo, J. J.; Lin, T.-A.; Perkinson, C. F.; Lu, Y.; Baldo, M. A.; Bawendi, M. G. Interfacial Trap-Assisted Triplet Generation in Lead Halide Perovskite Sensitized Solid-State Upconversion. *Adv. Mater.* **2021**, *33* (27), 2100854. https://doi.org/10.1002/adma.202100854.
(32) Bieber, A. S.; VanOrman, Z. A.; Wieghold, S.; Nienhaus, L. Perovskite-Sensitized Upconversion Bingo: Stoichiometry, Composition, Solvent, or Temperature? *J. Chem. Phys.* **2020**, *153* (8), 084703. https://doi.org/10.1063/5.0021973.

(33) Bieber, A. S.; VanOrman, Z. A.; Drozdick, H. K.; Weiss, R.; Wieghold, S.; Nienhaus, L. Mixed Halide Bulk Perovskite Triplet Sensitizers: Interplay between Band Alignment, Mid-Gap Traps and Phonons. *J. Chem. Phys.* **2021**. https://doi.org/10.1063/5.0077439.
(34) Droseros, N.; Dänekamp, B.; Tsokkou, D.; Boix, P. P.; Banerji, N. Charge Injection and Trapping at Perovskite Interfaces with Organic Hole Transporting Materials of Different Ionization Energies. *APL Mater.* **2019**, *7* (4), 041115. https://doi.org/10.1063/1.5086692.
(35) G. Stamplecoskie, K.; S. Manser, J.; V. Kamat, P. Dual Nature of the Excited State in Organic–Inorganic Lead Halide Perovskites. *Energy Environ. Sci.* **2015**, *8* (1), 208–215. https://doi.org/10.1039/C4EE02988G.
(36) Manser, J. S.; Kamat, P. V. Band Filling with Free Charge Carriers in Organometal Halide Perovskites. *Nat. Photonics* **2014**, *8* (9), 737–743. https://doi.org/10.1038/nphoton.2014.171.
(37) Xing, G.; Mathews, N.; Sun, S.; Lim, S. S.; Lam, Y. M.; Grätzel, M. Long-Range Balanced Electron- and Hole-Transport Lengths in Organic Inorganic CH3NH3PbI3. *Science* **2013**, *342*, 344–347.
(38) Chen, B. A.; Pang, G. T.; Lan, X. Q.; He, Z. B.; Chen, R. Strong Band Filling Induced Significant Excited State Absorption in MAPbI3 under High Pump Power. *Mater. Today Phys.* **2020**, *14*, 100228. https://doi.org/10.1016/j.mtphys.2020.100228.
(39) Anand, B.; Sampat, S.; Danilov, E. O.; Peng, W.; Rupich, S. M.; Chabal, Y. J.; Gartstein, Y. N.; Malko, A. V. Broadband Transient Absorption Study of Photoexcitations in Lead Halide Perovskites: Towards a Multiband Picture. *Phys. Rev. B* **2016**, *93* (16), 161205. https://doi.org/10.1103/PhysRevB.93.161205.
(40) Price, M. B.; Butkus, J.; Jellicoe, T. C.; Sadhanala, A.; Briane, A.; Halpert, J. E.; Broch, K.; Hodgkiss, J. M.; Friend, R. H.; Deschler, F. Hot-Carrier Cooling and Photoinduced Refractive Index Changes in Organic–Inorganic Lead Halide Perovskites. *Nat. Commun.* **2015**, *6* (1), 8420. https://doi.org/10.1038/ncomms9420.
(41) Bossanyi, D. G.; Sasaki, Y.; Wang, S.; Chekulaev, D.; Kimizuka, N.; Yanai, N.; Clark, J. In Optimized Rubrene-Based Nanoparticle Blends for Photon Upconversion, Singlet Energy Collection Outcompetes Triplet-Pair Separation, Not Singlet Fission. *J. Mater. Chem. C* **2021**. https://doi.org/10.1039/D1TC02955J.
(42) Ullah, M.; Yambem, S. D.; Moore, E. G.; Namdas, E. B.; Pandey, A. K. Singlet Fission and Triplet Exciton Dynamics in Rubrene/Fullerene Heterojunctions: Implications for Electroluminescence. *Adv. Electron. Mater.* **2015**, *1* (12), 1500229. https://doi.org/10.1002/aelm.201500229.
(43) Wu, T.; Ni, W.; Gurzadyan, G. G.; Sun, L. Singlet Fission from Upper Excited Singlet States and Polaron Formation in Rubrene Film. *RSC Adv.* **2021**, *11* (8), 4639–4645. https://doi.org/10.1039/D0RA10780H.
(44) Ma, L.; Galstyan, G.; Zhang, K.; Kloc, C.; Sun, H.; Soci, C.; Michel-Beyerle, M. E.; Gurzadyan, G. G. Two-Photon-Induced Singlet Fission in Rubrene Single Crystal. *J. Chem. Phys.* **2013**, *138* (18), 184508. https://doi.org/10.1063/1.4804398.
(45) Fu, J.; Xu, Q.; Han, G.; Wu, B.; Huan, C. H. A.; Leek, M. L.; Sum, T. C. Hot Carrier Cooling Mechanisms in Halide Perovskites. *Nat. Commun.* **2017**, *8* (1), 1300. https://doi.org/10.1038/s41467-017-01360-3.
(46) Lim, J. W. M.; Giovanni, D.; Righetto, M.; Feng, M.; Mhaisalkar, S. G.; Mathews, N.; Sum, T. C. Hot Carriers in Halide Perovskites: How Hot Truly? *J. Phys. Chem. Lett.* **2020**, *11* (7), 2743–2750. https://doi.org/10.1021/acs.jpclett.0c00504.

(47) Caselli, V. M.; Wei, Z.; Ackermans, M. M.; Hutter, E. M.; Ehrler, B.; Savenije, T. J. Charge Carrier Dynamics upon Sub-Bandgap Excitation in Methylammonium Lead Iodide Thin Films: Effects of Urbach Tail, Deep Defects, and Two-Photon Absorption. *ACS Energy Lett.* **2020**, *5* (12), 3821–3827. https://doi.org/10.1021/acsenergylett.0c02067.
(48) Kahmann, S.; Loi, M. A. Hot Carrier Solar Cells and the Potential of Perovskites for Breaking the Shockley–Queisser Limit. *J. Mater. Chem. C* **2019**, *7* (9), 2471–2486. https://doi.org/10.1039/C8TC04641G.
(49) Flender, O.; Klein, J. R.; Lenzer, T.; Oum, K. Ultrafast Photoinduced Dynamics of the Organolead Trihalide Perovskite CH3NH3PbI3 on Mesoporous TiO2 Scaffolds in the 320–920 Nm Range. *Phys. Chem. Chem. Phys.* **2015**, *17* (29), 19238–19246. https://doi.org/10.1039/C5CP01973G.
(50) Saeki, A.; Seki, S.; Takenobu, T.; Iwasa, Y.; Tagawa, S. Mobility and Dynamics of Charge Carriers in Rubrene Single Crystals Studied by Flash-Photolysis Microwave Conductivity and Optical Spectroscopy. *Adv. Mater.* **2008**, *20* (5), 920–923. https://doi.org/10.1002/adma.200702463.
(51) Dimitrov, S. D.; Wheeler, S.; Niedzialek, D.; Schroeder, B. C.; Utzat, H.; Frost, J. M.; Yao, J.; Gillett, A.; Tuladhar, P. S.; McCulloch, I.; Nelson, J.; Durrant, J. R. Polaron Pair Mediated Triplet Generation in Polymer/Fullerene Blends. *Nat. Commun.* **2015**, *6* (1), 6501. https://doi.org/10.1038/ncomms7501.
(52) Yang, Y.; Ostrowski, D. P.; France, R. M.; Zhu, K.; van de Lagemaat, J.; Luther, J. M.; Beard, M. C. Observation of a Hot-Phonon Bottleneck in Lead-Iodide Perovskites. *Nat. Photonics* **2016**, *10* (1), 53–59. https://doi.org/10.1038/nphoton.2015.213.
(53) Monahan, D. M.; Guo, L.; Lin, J.; Dou, L.; Yang, P.; Fleming, G. R. Room-Temperature Coherent Optical Phonon in 2D Electronic Spectra of CH3NH3PbI3 Perovskite as a Possible Cooling Bottleneck. *J. Phys. Chem. Lett.* **2017**, *8* (14), 3211–3215. https://doi.org/10.1021/acs.jpclett.7b01357.